# Ne II FINE-STRUCTURE LINE EMISSION FROM THE OUTFLOWS OF YOUNG STELLAR OBJECTS

Hsien Shang[1], Alfred E. Glassgold[2], Wei-Chieh Lin[1,3], and Chun-Fan J. Liu[1,3]

## ABSTRACT

The flux and line shape of the fine-structure transitions of Ne II and Ne III at 12.8 and $15.55\,\mu$m and of the forbidden transitions of O I $\lambda6300$ are calculated for young stellar objects with a range of mass-loss rates and X-ray luminosities using the X-wind model of jets and the associated wide-angle winds. For moderate and high accretion rates, the calculated Ne II line luminosity is comparable to or much larger than produced in X-ray irradiated disk models. All of the line luminosities correlate well with the main parameter in the X-wind model, the mass-loss rate, and also with the assumed X-ray luminosity — and with one another. The line shapes of an approaching jet are broad and have strong blue-shifted peaks near the effective terminal velocity of the jet. They serve as a characteristic and testable aspect of jet production of the neon fine-structure lines and the O I forbidden transitions.

*Subject headings:* ISM: jets and outflows – ISM: kinematics and dynamics – stars: formation – stars: low-mass – X-rays: stars

## 1. INTRODUCTION

More than 50 detections of the Ne II $12.8\,\mu$m line have been made in young stellar objects (YSOs) by the *Spitzer Space Telescope* (Espaillat et al. 2007; Lahuis et al. 2007; Pascucci et al. 2007; Ratzka et al. 2007; Carr & Najita 2008) and by ground based telescopes (Herczeg et al. 2007; Najita et al. 2009; van Boekel et al. 2009; Pascucci & Sterzik 2009). The neon fine-structure lines were predicted by Glassgold et al. (2007; henceforth GNI07) to arise in disk atmospheres irradiated by X-rays which ionize neon and generate the warm and high-ionization conditions needed to excite the lines. However, the formation of even a single low-mass star occurs in a multi-component system consisting of a collapsing cloud core, a disk, an accretion funnel and outflows arising close to the star. Thus various authors have suggested that the Ne II $12.8\,\mu$m line might be generated elsewhere in the system and not just by the disk (e.g., Meijerink et al. 2008, henceforth MGN08; Alexander 2008; van Boekel et al. 2009; Najita et al. 2009; Flaccomio et al. 2009; Guedel et al. 2010).

Information on the origin of the Ne II emission can be obtained from the velocity resolved profiles of the $12.8\,\mu$m line. Najita et al. (2009) discussed four such measurements: TW Hya (Herczeg et al. 2007); T Tau (van Boekel et al. 2009); AA Tau, and GM Aur (Najita et al. 2009). TW Hya and GM Tau are transitional disks, the former seen almost face-on and the latter at an inclination of 54°, whereas AA Tau is a classical T Tauri star (TTS) with a large inclination angle (75°). Pascucci & Sterzik (2009) have recently reported four more line shape measurements: TW Hya, T Cha, Sz 73, and CS Cha; T Cha, and CS Cha are also transitional

disks. Najita et al. (2009) concluded that the line profiles for TW Hya, AA Tau, and GM Aur are consistent with the emission arising mainly from a gravitationally bound disk atmosphere. Pascucci & Sterzik (2009) measured small blue shifts in three transition disks which they interpreted as arising from low-velocity ($\sim 10\,{\rm km\,s^{-1}}$) photo-evaporative outflows, following Alexander (2008). Observations of T Tau by van Boekel et al. (2009) show that the Ne II $12.8\,\mu$m emission in this case arises from more than one location within a complicated and only partially revealed triplet stellar system. T Tau is one of several accreting sources with very strong Ne II emission (Guedel et al. 2008). Its total Ne II luminosity is 20 times larger than measured for many revealed TTSs observed by *Spitzer*. The line shape of Sz 73 shows mainly blue-shifted emission extending well beyond $-100\,{\rm km\,s^{-1}}$, indicative of a strong stellar outflow. Neufeld et al. (2006) detected the Ne II $12.8\,\mu$m line in HH objects in the HH 7-11 outflow.

We show here that jets from YSOs, long known to emit the forbidden optical lines of heavy atomic ions, also generate the mid-infrared transitions of Ne II and Ne III. Using the X-wind model, we calculate the luminosities and shapes of these lines and also the forbidden O I $\lambda6300$ transitions for comparison. We obtain results for classical TTSs (Class I and II YSOs) with varying mass-loss rates, and we show that active jets can dominate the observed flux of the Ne II line. We also show that the line profiles have a distinctive shape that offers observational opportunities to verify the origin of the emission in strong outflow sources and to test the predictions of the X-wind model of jets.

## 2. METHODOLOGY

The X-wind theory of low-mass star formation (Shu et al. 1994) describes how the interaction of the magnetosphere and the accretion disk truncates the disk and forces its inner edge to co-rotate with the star. The interaction also drives an out-flowing wind and in-flowing accretion streams. In steady state, the inner edge of the disk coincides with the gravitational "X-point" of the system. Assuming that the flows emanate from this lo-

[1] Institute of Astronomy and Astrophysics (ASIAA), and Theoretical Institute for Advanced Research in Astrophysics (TIARA), Academia Sinica, P. O. Box 23-131, Taipei 10641, Taiwan
[2] Astronomy Department, University of California, Berkeley, CA 94720-3411, USA
[3] Graduate Institute of Astronomy and Astrophysics, National Taiwan University, No. 1, Sec. 4, Roosevelt Road, Taipei 10617, Taiwan

| Parameter | Symbol | Reference Case |
|---|---|---|
| Stellar mass | $M_*$ | $0.8\,M_\odot$ |
| Stellar radius | $R_*$ | $3.0\,R_\odot$ |
| Disk truncation radius | $R_{\rm x}$ | $4.8\,R_*$ |
| Stellar rotation period | $2\pi/\Omega_{\rm x}$ | $7.5\,{\rm d}$ |
| Wind mass-loss rate | $\dot{M}_{\rm w}$ | $1.6 \times 10^{-8}\,M_\odot\,{\rm yr}^{-1}$ |
| Disk accretion rate | $\dot{M}_{\rm d}$ | $1.2 \times 10^{-7}\,M_\odot\,{\rm yr}^{-1}$ |
| Mean terminal wind velocity | $\bar{v}_{\rm w}$ | $195\,{\rm km\,s}^{-1}$ |
| Stellar luminosity | $L_*$ | $2\,L_\odot$ |
| X-Ray luminosity | $L_{\rm X}$ | $3 \times 10^{31}\,{\rm erg\,s}^{-1}$ |
| Heating coefficient | $\alpha_h$ | $2 \times 10^{-3}$ |

cation allows a semi-analytic theory to be developed that yields a clear picture of outflows from low-mass YSOs. Shu et al. (1995) showed that the density asymptotes to cylindrical contours while the streamlines become radial. The physical conditions (temperature and ionization) of the X-wind were developed by Shang et al. (2002; henceforth SGSL) using Shang's (1998) semi-analytic representation of the flow. SGSL assumed the gas is atomic and heated by shocks and ionized by X-rays. They were able to give a good account of the optical observations of the forbidden lines and of the radio continuum observations of the Class I source, L1551 IRS 5 (Shang et al. 2004).

In addition to X-rays, SGSL considered a variety of heating and ionization sources (listed in their Table 1). For example, in addition to X-rays, they treated H$^-$ photo-detachment, Balmer continuum photoionization by stellar photons and by UV radiation from accretion-funnel hot spots, as well as collisional ionization. The X-rays can ionize a large part of the flow because radiative recombination occurs on a much longer time scale than the flow time scale (Bacciotti et al. 1995). Thus a significant level of ionization generated near the source of the flow is frozen into the wind out to larger distances. Many heating and cooling processes were considered, but SGSL found that the most important were: (1) adiabatic cooling of the expanding flow and (2) heating via the dissipation of internal velocity fluctuations and shocks. SGSL formulated the latter with a phenomenological formula for the mechanical heating rate per unit volume,

$$\Gamma = \alpha_h \frac{\rho v^3}{s}, \qquad (1)$$

where $\rho$ and $v$ are the local gas density and flow velocity, $s$ is the distance the fluid element has traveled along a streamline to the point of interest, and $\alpha_h \ll 1$ is a phenomenological coefficient that characterizes the magnitude of the mechanical heating. Equation (1) may be considered a prescription for shock heating in the jet. If velocity fluctuations of magnitude $\delta v$ generate the mechanical heating, then $\alpha_h v^3 \sim (\delta v)^3$, and the values of $\alpha_h$ needed to heat the flow, $\sim 0.001$, correspond to moderate velocity fluctuations, $\delta v/v \sim 0.1$. Values of this order may be inferred from high-spatial resolution observations of the optical forbidden lines emitted by revealed jets (e.g., Bacciotti et al. 2000; Woitas et al. 2002).

We use the SGSL model to calculate the neon fine-structure line emission for the wind and jet of a low-mass YSO. We also compare the neon lines with O I $\lambda 6300$, representative of optically forbidden lines. The results

depend on the model parameters listed in Table 1. The most important are the wind mass-loss rate and X-ray luminosity. In Table 1, both the wind mass-loss rate $\dot{M}_{\rm w}$ and the X-ray luminosity $L_{\rm X}$ are for a one-sided jet. The numerical values in the table are based on prior studies of jets (SGSL; Shang et al. 2004). We use the fiducial case of SGSL as our own reference model for a revealed T Tauri source that undergoes active accretion and drives a bright optical jet.

SGSL conceived the X-ray emission to arise from a soft coronal source of dimension $R_*$ enhanced by magnetic reconnection regions, one located in the disk midplane and two others associated with magnetic field $Y$-configurations above and below the plane (see the schematic drawing of Shu et al. 1997). They idealized this complex as a series of point sources, one at the origin and the others displaced along the axis at heights $\pm R_{\rm X}$ with $R_{\rm X} \sim 0.07\,{\rm AU}$. The total X-ray luminosity of each source was composed equally of soft and hard X-rays, described respectively by thermal spectra with $T_{\rm X} = 1\,{\rm keV}$ and $T_{\rm X} = 2\,{\rm keV}$. Because of the small dimensions of all of the sources ($\sim R_{\rm X}$), they behave much like a single coronal X-ray source with an additional hard component. The soft X-rays are absorbed over relatively short distances for outflows with appreciable mass loss. According to the reference model, the more penetrating hard X-rays irradiate one hemisphere with a luminosity, $L_{\rm X} \sim 1.5 \times 10^{31}\,{\rm erg\,s}^{-1}$.

The relatively large fiducial value of the X-ray luminosity in Table 1 was adopted by SGSL to treat active YSOs with bright jets and large accretion rates. Their conception of the X-ray properties of YSOs was formed by the results from the early X-ray observatories, *ASCA* and *ROSAT*, as discussed by Shu et al. (1997) who related the properties of the fluctuating X-wind model and the emission of X-rays. Following Shu et al. (1997), SGSL based their X-ray luminosity on *ROSAT* observations of embedded sources (Neuhäuser 1997), and took into account the likely effect of absorbing material close to the YSO that reduces the fraction of X-rays that escape to be detected by an X-ray observatory. Potentially an even more important absorber than the wind is the system of accretion columns, which carry a larger mass flux (e.g., Alexander et al. 2004, 2005). Screening by circumstellar material may help explain the long-standing puzzle concerning the larger X-ray luminosities of weak-lined versus classical TTSs, as suggested earlier by Gahm (1980) and by Walter & Kuhi (1981). Gregory et al. (2007) have demonstrated this effect by calculating the propagation of X-rays through the accretion funnels of a magnetospheric accretion model.

As discussed above, the calculations reported here cover a wide range of X-ray luminosities and not just the fiducial level in Table 1: $L_{\rm X}$ spans 3 orders of magnitude, from $L_{\rm X} = 3 \times 10^{29}$ to $L_{\rm X} = 3 \times 10^{32}$ ergs$^{-1}$. This range may be compared with the X-ray luminosities in the Guedel et al. (2010) correlation study of the Ne II line, where the measured X-ray luminosity varies over the range $\sim 10^{29} - 10^{31}\,{\rm erg\,s}^{-1}$. As we have just pointed out, it is difficult to make a direct connection between our model parameter $L_{\rm X}$ and measured X-ray luminosities. However, our main current goal is to deduce the overall trend of line luminosities with X-ray luminosity and not

detailed agreement for any particular object. This point is reinforced by the fact that the numerical results are affected by other model parameters which are not varied. For example, the effect of X-ray ionization at the base of the wind is affected by the location of our model point sources. Thus, if the elevated source is moved up in $z$, a smaller $L_X$ would be required to generate the same level of ionization.

## 3. RESULTS

Figure 1 shows the physical properties of the inner flow for the X-wind reference model in Table 1. The number density of atomic hydrogen is displayed with a color scale in Figure 1(a); the ordinate is the vertical distance $z$ and the abscissa is the cylindrical distance $\varpi$ in units of AU. Beyond $\varpi = 5\,\mathrm{AU}$, the density is approximately collimated cylindrically. The velocity field (solid lines) reaches near-terminal velocity within a few AU from launch and tends to be radial at large distances. The occurrence of a cylindrically stratified density in an expansive flow is characteristic of the magnetically collimated jet in the X-wind model.

The electron density is important for the production of the neon lines because the fine-structure transitions are excited by electron collisions. Figure 1(b) shows the electron density in color and the X-ray ionization rate $\zeta$ as solid black lines. Because the ionization tends to be frozen in, the electron density in the inner jet decreases more slowly with $\varpi$ than the ionization rate, which decreases rapidly due to absorption and inverse-square dilution of the X-rays. Both the electron density and the ionization rate manifest a conical shape similar to that often seen near the base of optical jets. Isotherms are also shown in Figure 1(b) as white lines. The magnitudes of the electron density and the temperature are suitable for exciting the neon lines. For example, the critical density of the Ne II $12.8\,\mu$m line is $4 - 5 \times 10^5\,\mathrm{cm}^{-3}$ for temperatures in the range $5,000 - 10,000\,\mathrm{K}$. In the very inner part of the jet, $\varpi < 2\,\mathrm{AU}$, the upper level of the transition is populated close to thermal equilibrium, but at larger distances the excitation is sub-thermal. For the reference case, most of the neon is ionized with roughly equal fractions in Ne$^+$ and Ne$^{++}$; Ne$^{++}$ gradually gives way to neutral neon at large distances along the innermost core of the jet, while it continues to account for $\sim 50\%$ of neon in the wide-angle wind.

We have calculated the luminosity of the neon lines for a range of models in which the main parameters, the X-ray luminosity $L_X$ and the mass-loss rate $\dot{M}_w$ both for a one-sided jet are varied away from the reference values in Table 1. In some cases, their *ratio* is kept fixed at $L_X/\dot{M}_w = 3 \times 10^{13}\,\mathrm{erg\,g}^{-1}$, while the wind mass-loss rate changes from $5 \times 10^{-7}$ to $5 \times 10^{-10}\,M_\odot\,\mathrm{yr}^{-1}$. This range extends from a somewhat embedded Class I source down to the level of a revealed classical TTS. Line fluxes are calculated for the standard sequence of parameters used by Shang et al. (2004). Then the mass-loss rates are increased and decreased by factors of 3 keeping $L_X/\dot{M}_w$ fixed. Finally, the constraint of fixed $L_X/\dot{M}_w$ is removed for each of these standard cases, and $L_X$ is varied by 1 order of magnitude above and below the standard series.

The ionization balance of the neon species is calculated by the method given in Section 2 of GNI07. Excitation by neutral hydrogen has been ignored because the large electron fractions make electron collisions dominant. The total abundance of neon is set at $10^{-4}$ relative to hydrogen and that of oxygen at $6.6 \times 10^{-4}$, following the discussion in GNI07. The populations of the lowest five levels of Ne$^{++}$ and O I were solved exactly as were the two levels for Ne$^+$. The lines were assumed to be optically thin, a good approximation for the region shown in Figure 1.

Figure 2 plots the luminosity of the Ne II $12.8\,\mu$m and Ne III $15.55\,\mu$m lines and the forbidden transitions of O I $\lambda6300$ against three variables: (a) the mass-loss rate $\dot{M}_w$, (b) the X-ray luminosity $L_X$, and (c) the product $L_X\dot{M}_w$ — introduced by Guedel et al. (2008) in a search for empirical correlations of the Ne II luminosity with other properties of YSOs. Values from both groups of calculations (fixed and variable $L_X/\dot{M}_w$) are plotted. The fluctuations in Figures 2(a) and (b) show the effects of the variable not plotted. The quantity $\dot{M}_w$ is intrinsic to X-wind theory, whereas $L_X$ is an external parameter that was added in the development of the physical properties of the X-wind by SGSL. There is no self-consistent theory available yet that treats both the magnetospheric wind and accretion generation together with X-ray emission. The heating coefficient $\alpha_h$ in Equation 1 is another external parameter introduced by SGSL, but it is less effective in changing the physical properties of the outflow, and for purposes of simplicity it is not varied very far from the value in Table 1 for the reference model. The large open triangles in Figure 2 are for the reference case. The model calculations all fit power laws with relatively small scatter, i.e., the $3\sigma$ uncertainties in the least-square slopes are all significantly smaller than the slopes themselves. The parameter $\alpha_h$ has been kept fixed at 0.002 in Figure 2; varying $\alpha_h$ by a factor of a few would naturally introduce some scatter without changing the slope. Unlike the case of disk emission (MGN08), the correlation with X-rays in Figure 2(b) is reasonably well founded because the effects of the other main parameter $\dot{M}_w$ are seen in Figure 2(b) to be relatively modest.[4]

Somewhat surprisingly, the fits with the empirical parameter $L_X\dot{M}_w$ in Figure 2 are superior to the other two. The ratio of the $1\sigma$ uncertainty in slope to the slope itself is $\sim 0.05$. A possible interpretation of this correlation is that it reflects the primary role of the electron density in producing the neon ions and in exciting their line emission. This in turn follows from the idea that $L_X/\dot{M}_w$ is the global average of the local X-ray radiation parameter, $\zeta/n$. This quantity is roughly proportional to the square of the electron fraction, so that the square root of the empirical parameter, $L_X\dot{M}_w$, is a measure of the *electron density*.

The slope of the correlations for O I in Figure 2 is larger than those of the Ne II and Ne III lines, and the Ne II slope may be slightly larger than the one for Ne III. These differences can be traced to the ionization fractions of these

---

[4] Figure 2(b) is similar to Figure 16 of MGN08, where the luminosity of several diagnostic lines, including the Ne II $12.8\,\mu$m line, are plotted versus $L_X$ for the same disk structure, that of a generic TTS disk. A correlation diagram for a real sample of observed TTS disks may not follow this power law because it will likely include a variety of disks at different ages and density structures.
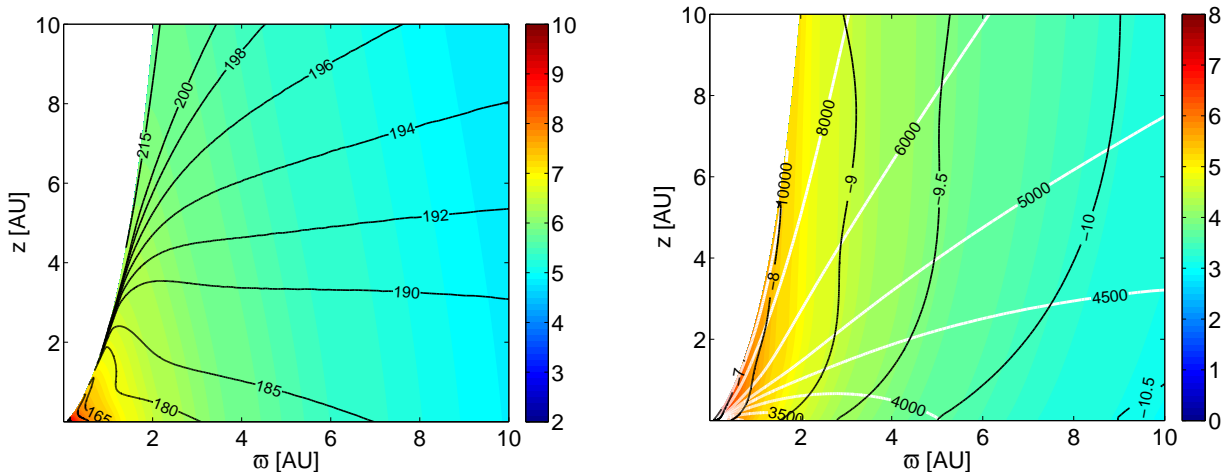
FIG. 1.— (a) Background density of atomic hydrogen (color scale) and velocity contours (solid black lines) for the X-wind reference case. (b) Electron density (color scale), ionization rate $\zeta$ (solid black lines) and temperature (white lines). Volumetric densities are given in cgs units and velocities in km s$^{-1}$.

ions. As pointed out by MGN08, direct ionization of neutral oxygen by X-rays is not competitive compared with charge exchange with H$^+$. As a result, the neutral oxygen fraction in the present calculations is above 90% except for very small values of $L_{\rm X}$ and $\dot{M}_{\rm w}$. On the other hand, the Ne$^+$ and Ne$^{++}$ fractions are sensitive to the local X-ray ionization parameter, $\zeta/n$. Thus for the reference case, the Ne$^{++}$/Ne$^+$ ratio approaches unity in the inner jet, but then falls to $\sim 0.5$ throughout the rest of inner region of the outflow ($\varpi < 10\,{\rm AU}$) due to attenuation and inverse-square dilution of the X-ray flux. For larger values of $\dot{M}_{\rm w}$, attenuation takes an increasing toll and reduces the Ne$^{++}$/Ne$^+$ ratio, although it is always larger in the inner jet than in the outflow at large. This explains the tendency of the luminosity ratio $L({\rm Ne\,III})/L({\rm Ne\,II})$ in Figures 2(a) and (c) to decrease with increasing $\dot{M}_{\rm w}$. This tendency is at most moderately significant because of the large fluctuations in the theoretical predictions of the luminosities of the Ne II and Ne III lines in Figure 2.

The fact that the luminosities in Figure 2 correlate well with the variables $\dot{M}_{\rm w}$ and $L_{\rm X}$ means that they correlate with one another. This is illustrated in Figure 3, where the Ne II 12.8 $\mu$m luminosity is plotted against the O I $\lambda 6300$ luminosity on a log-log scale. The slope of the correlation line is $0.83 \pm 0.048$. The O I $\lambda 6300$ lines have long been used as diagnostics of YSO jets. The predicted correlation with Ne II suggests that the latter line may also be a good diagnostic for these jets. Because our calculations are based on X-wind theory supplemented by chemical-physical considerations, including X-ray ionization of the outflow, Figure 3 offers a potentially useful observational test of the excitation theory in SGSL without the uncertainties of external parameters such as $L_{\rm X}$. A preliminary inspection of the available data for jet sources in Guedel et al. (2010) suggests a good correlation with our theory. Further detailed comparisons of the Ne II 12.8 $\mu$m and the O I $\lambda 6300$ luminosities should be helpful in understanding the origin of these emission lines.

Figure 4(a) shows normalized profiles of the Ne II 12.8 $\mu$m, Ne III 15.55 $\mu$m and the O I $\lambda 6300$ lines for the reference case of Table 1 at an inclination angle of 45°. The calculations are for one side of the outflow and the results have been binned to a spectral resolution of 1 km s$^{-1}$. The predicted emission extends over a broad range of velocities from $\sim -200$ to $\sim +100$ km s$^{-1}$ at this inclination, The dominant feature is the large blue-shifted peak close to the projected terminal velocity of the jet. Figure 4(b) shows the contributions to the Ne II line shape as a function of the cylindrical coordinate $\varpi$. As $\varpi$ increases, the height of the peak grows from contributions of regions with ever-increasing radius and outflow velocities close to the terminal value. The Ne II line has a broader low-velocity wing than the other lines, indicating that Ne II fraction is more sensitive to the physical conditions close to the source and the acceleration zone. On a larger scale, the Ne II line is generated at relatively small distances, $\varpi < 5\,{\rm AU}$, with the broad wing from $\sim -50$ to $\sim +50$ km s$^{-1}$ produced within $\sim 1 - 2\,{\rm AU}$ of the axis. This is close to the source of the wind; Figure 1(a) shows that the wind velocity is already quite large by $z = 0.5\,{\rm AU}$.

The line profiles vary with the inclination angle, which is important for making comparisons with observations. Figures 5(a) and (b) show line shapes at 30° and 60° for one side of the jet; they are similar to the 45° case shown in Figure 4(a). Significant changes occur for inclinations near 90° and 0°. Near these extremes, the emission peak occurs close to the real terminal velocity for the face-on case (0°), while it approaches the stellar velocity for the edge-on case (90°). The X-wind jet flow has the form of a cylindrically symmetric rounded cone or bowl. The peak velocity in the emission is determined by the projection of the terminal velocity. The line shape varies gradually with inclination angle as the projected velocity peak moves toward larger or smaller projected values. The low velocity wing remains broad and extends to negative velocities. In theory, the jet is bipolar, and the full profiles are in principle symmetric with respect to the stellar velocity. The receding jet produces a red-shifted emission peak at the same magnitude of projected velocity as the blue-shifted peak, and its low-velocity wing extends to the blue. Depending on the actual viewing angle and orientation of the system, the line profile of a jet with two visible lobes will be a mixture of shapes from each
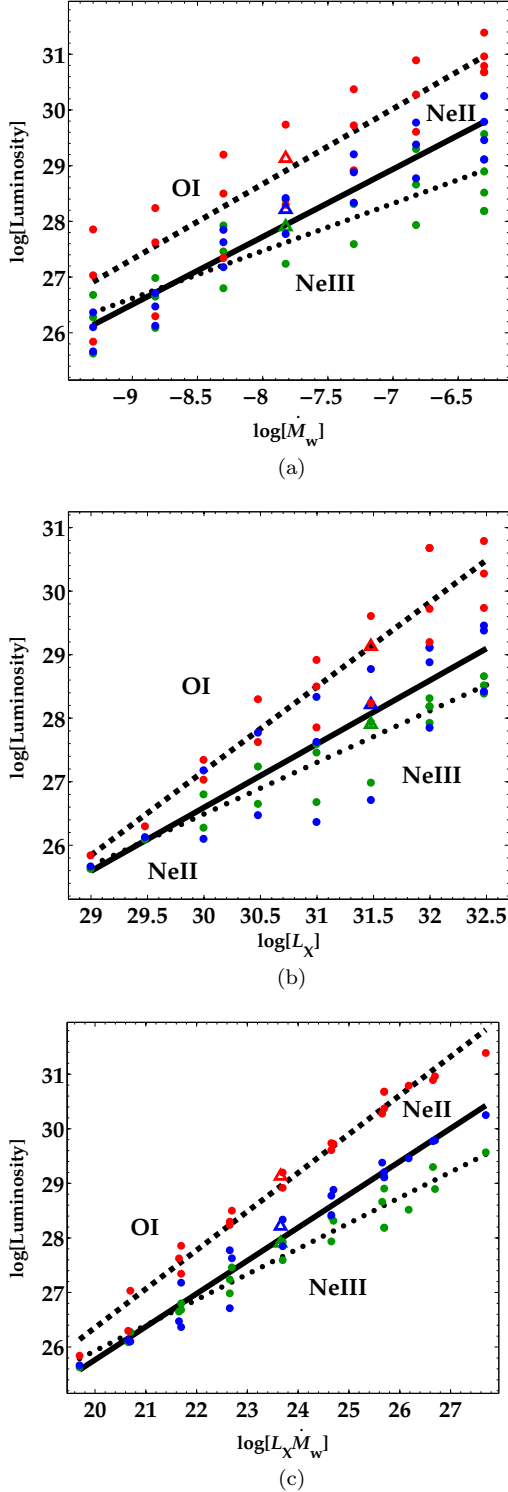
(a)

(b)

(c)

FIG. 2.— (a) Line luminosities Ne II 12.8 $\mu$m (solid line), Ne III 15.55 $\mu$m (dotted line), and the O I $\lambda$6300 (dashed line) from a one-sided jet, plotted versus $\dot{M}_{\rm w}$ in units of $M_\odot$ yr$^{-1}$. The vertical axis labels line luminosities in erg s$^{-1}$. The open triangles mark the reference case of Table 1. $\dot{M}_{\rm w}$ is the mass-loss rate from one hemisphere. The slopes of the power-law fits are: $1.351 \pm 0.132$ (O I); $1.215 \pm 0.084$ (Ne II); $0.851 \pm 0.110$ (Ne III). (b) Same as (a), except the line luminosities are plotted versus the X-Ray luminosity $L_{\rm X}$ of a one-sided jet in units of erg s$^{-1}$. The slopes of the power-law fits are: $1.328 \pm 0.117$ (O I); $1.001 \pm 0.152$ (Ne II); $0.813 \pm 0.068$ (Ne III). (c) Same as (a), except the line luminosities are plotted versus $L_{\rm X}\dot{M}_{\rm w}$ in units of erg s$^{-1}$ $\times$ $M_\odot$ yr$^{-1}$. The slopes of the power-law fits are: $0.709 \pm 0.022$ (O I); $0.606 \pm 0.026$ (Ne II); $0.468 \pm 0.022$ (Ne III).
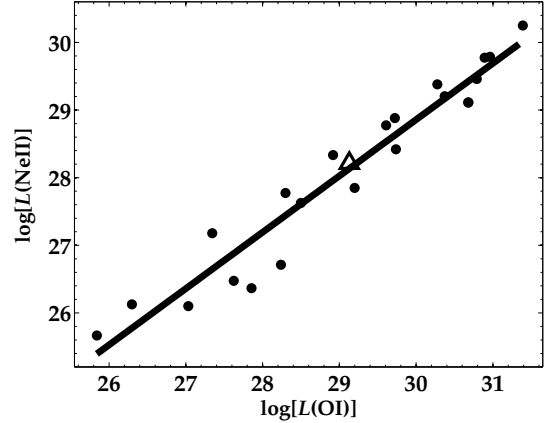


FIG. 3.— Luminosity of the Ne II 12.8 $\mu$m line vs. the O I $\lambda$6300 luminosity in a log-log plot; the units are erg s$^{-1}$. The correlation line has a slope close to 0.8.

side. If for some reason only the receding side is visible, the profile will be peaked at the high red-shifted velocity. Several authors have suggested that sources with observed high Ne II luminosity are associated with jets (e.g., Guedel et al. 2010; van Boekel et al. 2009; Flaccomio et al. 2009). Our results support this view, and our specific predictions can be checked by the detection of strong blue-shifted line emission, as seen in Figures 4 and 5.

## 4. DISCUSSION AND CONCLUSIONS

We have calculated the emission of the Ne II 12.8 $\mu$m, Ne III 15.55 $\mu$m and O I $\lambda$6300 lines for the X-wind model for the outflows from YSOs. The oxygen lines are well-established diagnostics of jets, whereas the Ne II 12.8 $\mu$m line has only recently become a probe of the circumstellar gas of young stars, as described in the Introduction. We have calculated the dependence of the line emission on the two main parameters of the model, the wind mass-loss rate $\dot{M}_{\rm w}$ and the X-ray luminosity $L_{\rm X}$. The mass-loss rate is an intrinsic parameter of X-wind theory, whereas the X-ray luminosity was added by SGSL in modeling the physical properties of the wind. Figure 2(a) expresses our first basic result. It shows that the line luminosities correlate well with the X-wind parameter $\dot{M}_{\rm w}$. Figure 2(a) also shows that, for mass-loss rates in excess of those characteristic of Class II TTSs, the luminosity of the Ne II 12.8 $\mu$m is well above the observed range for this line given by Guedel et al. (2010). It is interesting that the combination parameter, $L_{\rm X}\dot{M}_{\rm w}$, gives the best correlation of the three shown in Figure 2. Figure 3 gives another example of a good correlation, in this case between the O I forbidden transitions and the Ne II fine-structure line. It suggests that the Ne II 12.8 $\mu$m line is an excellent probe of the jets from YSOs, as are of course the well-established O I $\lambda$6300 line.

The theoretical line profiles displayed in Figures 4 and 5 have a distinctive shape. For an approaching one-sided jet, they have a strong blue-shifted peak near the wind terminal velocity that is associated mainly with the inner part of the jet within $\varpi < 5$ AU. There is also a broad shoulder centered around the stellar velocity that arises near the source of the jet and the acceleration region of the outflow. These features reflect some of the unique properties of the X-wind model of outflows from YSOs.
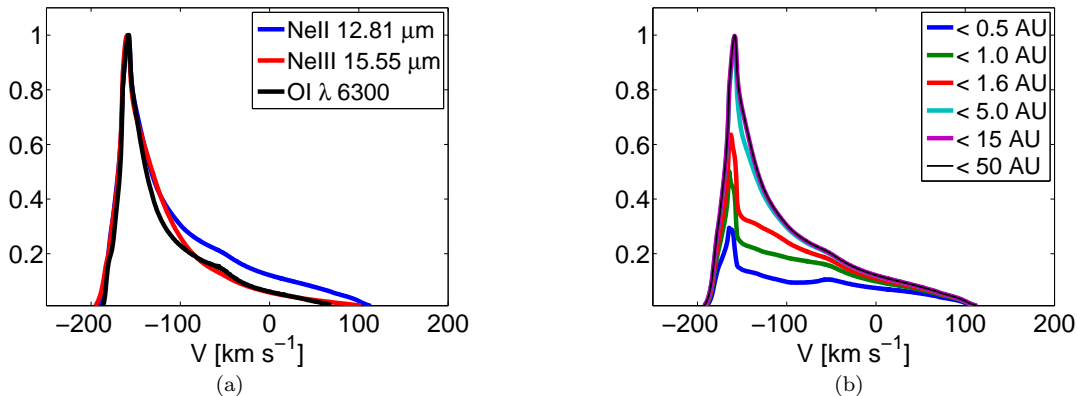
FIG. 4.— (a) Line profiles for Ne II 12.8 $\mu$m (blue), Ne III 15.55 $\mu$m line (red) and the O I $\lambda$6300 (black) for the X-wind jet, calculated for the reference case of Table 1. The inclination angle is 45°, and the line shapes are normalized to their peak values. (b) Buildup of the Ne II line shape as a function of cylindrical radius $\varpi$ for the case of 45° inclination angle.
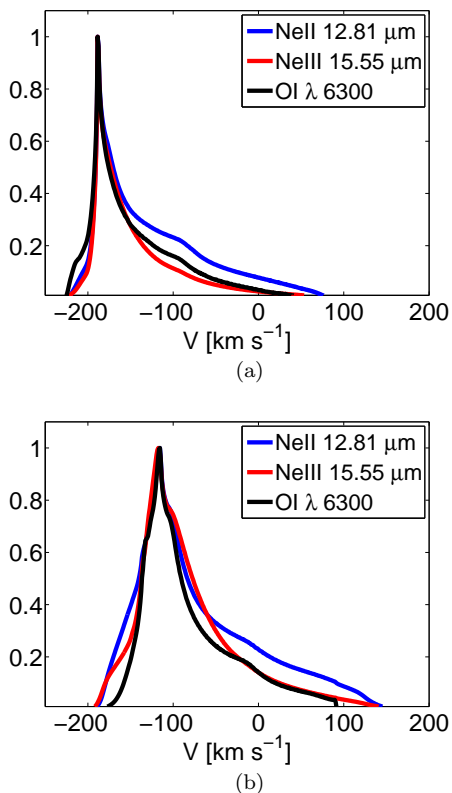


FIG. 5.— (a) Line profiles for Ne II 12.8 $\mu$m (blue), Ne III 15.55 $\mu$m line (red) and the O I $\lambda$6300 (black) for the approaching X-wind jet, calculated for the reference case of Table 1. The inclination angle is 30°, and the line shapes are normalized to their peak values. (b) Line profiles for Ne II 12.8 $\mu$m (blue), Ne III 15.55 $\mu$m line (red) and the O I $\lambda$6300 (black) for the X-wind jet, calculated for the reference case of Table 1. The inclination angle is 60°, and the line shapes are normalized to their peak values.

Observations to test these predictions for high luminosity sources are feasible for both the Ne II 12.8 $\mu$m and the O I $\lambda$6300 lines. High-spectral resolution measurements would be of great interest for understanding the source of the Ne II and O I line emission, the role of X-rays in determining the physical properties of outflows, and the dynamics of jet formation. The blue-shifted peak of the Ne II line is probably the most important signature of jet emission, because the low-velocity shoulder may be contaminated in some cases by emission from the X-ray

irradiated disk, either from the disk proper (MGN08) or from a photo-evaporated wind (Owen et al. 2010; Ercolano & Owen 2010).

Line profile measurements have already been carried out for seven low-mass YSOs, as discussed in the Introduction. Four of the seven are transition objects which have evolved disks with substantial gaps in the inner dust distribution (TW Hya, GM Aur, CS Cha, and T Cha), typically on the AU scale. These four objects all show clear signatures of accretion onto the stellar surface, which implies that there is a significant amount of gas present within the inner radius of the dust gap. These are not the most appropriate systems for applying the X-wind model, originally conceived to describe YSOs with strong outflows. Two of the seven YSOs (T Tau and Sz 73) are outflow sources. The simple X-wind model used in this paper is inadequate to deal with the T Tau triple stellar system, which has multiple sources of X-rays and Ne II line emission. Of all the line shapes reported by Pascucci & Sterzik (2009), the broad, blue-shifted line of Sz 73 is closest to the profiles we show in Figures 4 and 5. However, little is known about this YSO, and it would be premature to conclude that it agrees (or disagrees) with our model until more information is obtained, e.g, its X-ray properties determined, and detailed modeling is carried out. This leaves AA Tau, whose line shape has been measured by Najita et al. (2009) to be broad (FWHM $\sim 70\,\mathrm{km\,s^{-1}}$) and with a red-shifted peak at $+15\,\mathrm{km\,s^{-1}}$. There is also emission corresponding to the blue-shifted velocity, but the spectrum is noisy and difficult to characterize. With its large inclination angle, it is possible that higher signal-to-noise observations may show the line shape expected on the basis of our X-wind calculations, especially since AA Tau manifests some evidence for outflow (Bouvier et al. 2003, 2007). On the other hand, the flux of its Ne II 12.8 $\mu$m line is at the level obtained for X-ray irradiated disk models (MGN08). Thus any serious model calculation would have to include all the sources of emission, the accretion funnel, the disk and the wind. We would like to recommend that searches be made for Ne II 12.8 $\mu$m line emission from strong jets already detected in forbidden transitions from O I and other heavy ions using high-resolution MIR spectrometers on large telescopes.

Hollenbach & Gorti (2009) have provided an alternative view of the Ne II 12.8 $\mu$m line emission for sources

with high accretion rates. In their theory, the main source of ionization of neon and the excitation of the 12.8 $\mu$m line is high-velocity ($\sim 100\,\mathrm{km\,s^{-1}}$) shocks that affect the entire jet. While high-velocity shocks may generate large enough temperatures to ionize neon in localized regions, there is little observational evidence for the strong and continuous shocking of jets. The bulk of the magnetized flow is at most mildly shocked, despite the high terminal speeds reached close to the source. It is these mild shocks that are responsible for heating the outflow in the present model. Hollenbach & Gorti (2009) do not calculate line shapes for their high-velocity shock model. Although they are likely to be broad ($\sim 100\,\mathrm{km\,s^{-1}}$), the line shapes can be expected to be different from the ones shown here because the broadening arises downstream along the jet where the strong shocks occur. In contrast, most of the Ne II and Ne III emission in our work is generated within or close to the acceleration region that surrounds the source, so that the line shape takes its final form close to the source, as shown in Figure 4.

Guedel et al. (2010) have made extensive searches for observational correlations of the Ne II 12.8 $\mu$m line luminosity with X-ray luminosity and other properties of YSOs, as have Flaccomio et al. (2009). They do not find any particular trend for low-accretion systems, where the measured Ne II luminosities span a range of a factor of 10 or more about a median of approximately $L(\mathrm{Ne\,II}) \cong 5 \times 10^{-6}\,L_\odot$ (or $\log L(\mathrm{Ne\,II}) = 28.25$ in cgs units). This value is close to our reference theoretical value, the large open triangle in Figure 2. It is also similar to the value predicted by MGN08 for an X-ray irradiated disk of a typical TTS, although the Ne II emission from disks has not been calculated for any other case. Calculations for photo-evaporated winds give similar values (Alexander 2008; Ercolano & Owen 2010). One explanation for the large number of measurements for both optically thick and transition disks with this level of Ne II luminosity is that other variables are important, and not just the X-ray luminosity. Schisano et al. (2010) illustrate this possibility by showing that variations in disk flaring and X-ray spectrum give rise to a scatter in the predicted Ne II luminosity similar to what is observed. According to our calculations, outflows may also contribute in some cases, but they are not the dominant source of emission for low or even moderate accretion rates and X-ray luminosities. However, as shown in Figure 2, they may dominate for high mass-loss rates and X-ray luminosities. Thus our calculations support the "bi-modal" picture of Guedel et al. (2010) and van Boekel et al. (2009), especially their suggestion that the Ne II luminosity of high-accretion sources arises in outflows.

On the basis of a regression analysis, Guedel et al. (2010) also concluded that the Ne II luminosities of jet sources correlate, not only with X-ray luminosity, but with accretion rate and mass-loss rate. The significance of these correlations is diminished by the relatively small sample of sources for which the parameters have been measured and by scatter in the data. This is especially true in the case of the mass-loss rate, where only two sources (T Tau N and DG Tau) have exceptionally large Ne II luminosities. Without relying on these two "out-

liers",[5] the correlation of the Ne II luminosity with mass-loss rate is not yet definitively established. Such a correlation would be directly relevant to the present calculations because, in X-wind theory, it is the mass-loss rate that directly determines the properties of the outflow, rather than the accretion rate, although the two are related. Mass-loss rates of YSO jets are often determined from bright optical emission lines such as O I $\lambda$6300 (e.g., Hartigan et al. 1994, 1995), but the results for YSOs of the same mass can range over several dex (White & Hillenbrand 2004). In light of such uncertainties, it would be better to compare the luminosity of the O I $\lambda$6300 with that of the Ne II line, as we do in Figure 3. Guedel et al. (2010) test this correlation with data for sources they identify as optically thick disks without jets, transition disks, and jet sources. A preliminary inspection of the available data for the seven jet sources in their Figure 4 with $L(\mathrm{Ne\,II}) > 8 \times 10^{-6}\,L_\odot$ suggests a good correlation with our theory. Further observations of the Ne II and O I emission from strong jets including line shape measurements would be extremely useful in this connection.

The correlation predictions in Figure 2 suggest another possible test of our calculations using the Ne III 15.55 $\mu$m line, although only a few detections of this line have been reported so far. In Figure 2(a) the predicted but uncertain ratio of the Ne II 12.8 $\mu$m to the Ne III 15.55 $\mu$m line flux is in the range $\sim 1-10$; the Ne III flux is $\sim 10^{-14} - 10^{-13}\,\mathrm{erg\,cm^{-2}\,s^{-1}}$. Lahuis et al. (2007) reported a tentative detection of the Ne III line with *Spitzer* for Sz 102, a poorly studied source with a prominent jet, known to emit primarily soft X-rays (Guedel et al. 2010). Lahuis et al. (2007) give the neon line fluxes as $L(\mathrm{Ne\,II}) = 3.6 \times 10^{-14}\,\mathrm{erg\,cm^{-2}\,s^{-1}}$ and $L(\mathrm{Ne\,III}) = 2.3 \times 10^{-15}\,\mathrm{erg\,cm^{-2}\,s^{-1}}$, or a Ne III/Ne II luminosity ratio of $\sim 1/16$. This small value is consistent with a disk origin for the neon lines, but the measured fluxes are smaller than predicted by MGN08 for the generic TTS disk and the measured X-ray luminosity. Flaccomio et al. (2009) detected both neon lines from the F7 Class III YSO WL5/GY246 in the $\rho$ Oph cluster. Although the luminosities are in rough accord with a disk origin, the Ne III/Ne II luminosity ratio of $\sim 1/4$ is somewhat higher than given by MGN08 and more like the values obtained here for jets. However, we would not expect to find a strong jet in a Class III YSO, so the disk model is favored in this case. A careful determination of upper limits if not detections in *Spitzer* spectra of high luminosity sources of the Ne III 15.55 $\mu$m line could provide further checks of our theory. Since *Spitzer* operations have entered the warm phase, further direct detections of this line from space will not be available for some time. However the optical lines of Ne III $\lambda$3869/3967 are accessible from the ground, and they have been observed from H II regions and other highly-ionized sources. Preliminary calculations indicate that these lines have about the same luminosity as the Ne III 15.55 $\mu$m line. We suggest that these lines be used to further probe the ionization state and emission characteristics of jets and disks around low-mass YSOs.

In conclusion, we have calculated the emission of the fine-structure lines of neon and of the forbidden O I tran-

---

[5] T Tau N is an outlier in that it is part of a compact triple system; DG Tau has an unusually small *observed* X-ray luminosity.

sitions near 6300 Å, according to the X-wind model of jets. These lines trace similar aspects of the outflow. They correlate well with the X-wind model parameters and with the combination variable $L_{\rm X}\dot{M}_{\rm w}$, as well as with one another. We have suggested several tests of the calculations, including the measurement of the unique blue-shifted peak in the line profile near the wind terminal velocity. We also suggest that jets may account for the luminous mode in the bimodal picture of Ne II correlations proposed by Guedel et al. (2010) and van Boekel et al. (2009).

## REFERENCES

Alexander, R. D. 2008, MNRAS, 391, L64

Alexander, R. D., Clarke, C., & Pringle, J. 2004, MNRAS, 348, 879

Alexander, R. D., Clarke, C., & Pringle, J. 2005, MNRAS, 358, 283

Bacciotti, F., Chiuderi, C., & Oliva, E. 1995, A&A, 296, 185

Bacciotti, F., Mundt, R., Ray, T. P., Eislöffel, J., Solf, J., & Camenzind, M. 2000, ApJ, 537, L49

Bouvier, J., et al. 2003, A&A, 409, 169

Bouvier, J., et al. 2007, A&A, 463, 1017

Carr, J. S., & Najita, J. R. 2008, Science, 319, 1504

Ercolano, B., & Owen, J. E. 2010, MNRAS, in press (arXiv: 1004.1203)

Espaillat, C., et al. 2007, ApJ, 664, L111

Flaccomio, E., Stelzer, B., Sciortino, S., Pillittieri, & Testi, L. 2009, A&A, 505, 695

Gahm, G. F. 1980, ApJ, 242, L163

Glassgold, A. E., Najita, J., & Igea, J. 2007, ApJ, 656, 515 (GNI07)

Gregory, S. G., Wood, K., & Jardine, M. 2007, MNRAS, 379, L35

Guedel, M., et al. 2008, http://www.ipac.caltech.edu/spitzer2008

Guedel, M., et al. 2010, A&A, in press

Hartigan, P., Edwards, S., & Ghandour, L. 1995, ApJ, 452, 736

Hartigan, P., Morse, J. A., & Raymond, J. 1994, ApJ, 436, 125

Herczeg, G. J., Najita, J. R., Hillenbrand, L. A., & Pascucci, I. 2007, ApJ, 670, 509

Hollenbach, D., & Gorti, U. 2009, ApJ, 703, 1203

Lahuis, F., Van Dishoeck, E. F., Blake, G. A., Evans, N. J., II, Kessler-Silacci, J. E., & Pontoppidan, K. M. 2007, ApJ, 665, 492

Meijerink, R., Glassgold, A. E., & Najita, J. R. 2008 ApJ, 676, 518 (MGN08)

Najita, J. R., et al. 2009, ApJ, 697, 957

Neufeld, D. A., et al. 2006, ApJ, 649, 816

Neuhäuser, R. 1997, Science, 276, 1363

Owen, J. E., Ercolano, B., Clarke, C. J., & Alexander, R. D. 2010, MNRAS, 401, 1415

Pascucci, I., et al. 2007, ApJ, 663, 383

Pascucci, I., & Sterzik, M. 2009, ApJ, 702, 724

Ratzka, Th., Leinert, Ch., Henning, Th., Bouwman, J., Dullemnond, C. P., & Jaffe, W. 2007, A&A, 471, 173

Schisano, E., Ercolano, B., & Guedel, M. 2010, MNRAS, 401, 1636

Shang, H. 1998, PhD. thesis, Univ. California, Berkeley

Shang, H., Glassgold, A. E., Shu, F. H., & Lizano, S. 2002, ApJ, 564, 853 (SGSL)

Shang, H., Lizano, S., Glassgold, A. E., & Shu, F. 2004, ApJ, 612, L69

Shu, F. H., Najita, J., Ostriker, E. C., & Shang, H. 1995, ApJ, 455, L155

Shu, F. H., Najita, J., Ostriker, E. C., Wilkin, F., Ruden, S., & Lizano, S. 1994, ApJ, 429, 781

Shu, F. H., Shang, H., Glassgold, A. E., & Lee, T. 1997, Science, 277, 1475

van Boekel, R., Guedel, M., Henning, Th., Lahuis, F., & Pantin, E. 2009, A&A, 497, 137

Walter, F. M., & Kuhi, L. V. 1981, ApJ, 250, 254

White, R. J., & Hillenbrand, L. A. 2004, ApJ, 616, 998

Woitas, J., Ray, T. P., Bacciotti, F., Davis, C. J., & Eislöffel, J. 2002, ApJ, 580, 336